Materials Science Forum
ISSN: 1662-9752, Vol. 1183, pp 25-33
doi:10.4028/p-IZfbh8

Submitted: 2026-01-16
Revised: 2026-02-17
Accepted: 2026-02-24
Online: 2026-04-13

Characterisation of the Flow Behaviour of Powder Metallurgical Semi-Finished Products for Lubricant-Impregnated Cold Forming Concepts

Prajapati Kishan Rahul[1,a*], Laeger René[1,b], Mohnfeld Norman[1,c], Peddinghaus Julius[1,d], Uhe Johanna[1,e] and Behrens Bernd-Arno[1,f]

[1]Leibniz University Hannover, Institute of Forming Technology and Machines, An der Universität 2, 30823 Garbsen, Germany

[a*]prajapati@ifum.uni-hannover.de, [b]laeger@ifum.uni-hannover.de, [c]mohnfeld@ifum.uni-hannover.de, [d]peddinghaus@ifum.uni-hannover.de, [e]uhe@ifum.uni-hannover.de, [f]behrens@ifum.uni-hannover.de

*corresponding author: prajapati@ifum.uni-hannover.de

Keywords: powder metallurgy, characterisation, flow behaviour, porosity.

Abstract. In cold bulk metal forming, coatings based on zinc phosphate are commonly used for lubrication. This has a negative impact on the environment, negatively affects human health, and requires significant pre- and post-surface treatments. Powder metallurgical (PM) components are a promising alternative to zinc phosphate coatings due to the process related porosity of the workpiece which acts as lubricant reservoir. During the forming process, the lubricant stored in the pores is released and lubricates the tool and workpiece surfaces. For an efficient process design of such components, finite element method (FEM) is an effective tool to analyse forming and friction behaviour. To this end, a realistic material model is essential for accurate simulation results. Hence, in this work, the flow behaviour of PM semi-finished products is characterised by means of compression and tensile tests. The results indicate that the material exhibits different behaviour under compression and tension. In compression, the material demonstrates higher yield strength and flow stresses compared to tension. Additionally, inhomogeneity of the material distribution can be observed, characterised by a denser core and more porous outer regions. The porous outer regions make it suitable for storing lubricant for application in forming processes.

Introduction

The growing concern regarding industrial application of hazardous lubricants is highlighted by new legislations such as Registration, Evaluation, Authorisation and Restriction of Chemicals [1]. Due to these legislations, there has been an increased focus on environmental and human health from the risk posed by these chemicals. In cold forming, lubrication is essential to increase the tool life and reduce forming forces [2]. In cold bulk metal forming, the surface expansion can reach values up to 3,000%, leading to a need for conversion layers as lubricant carrier [3]. Coatings based on zinc phosphate are commonly used for this application. The coating procedure has several environmental drawbacks such as sludge of heavy metal phosphates that needs to be reclaimed or buried, large amount of water requirement in rinse baths and high quantities of waste water typically containing grease, oil, acid, and soap [4]. Furthermore, the coating process requires significant pre-surface treatments such as shot blasting and pickling to prepare surface for adhesion of coatings [3, 5]. This leads to higher costs and energy requirements for the lubrication process.

As an alternative to zinc phosphate coatings, several options have been developed. Electrolytic phosphating developed by Bjerrum et al. does not produce heavy metal sludge in baths and avoids the use of acid by electrochemical pickling compared to the chemical phosphating process [6]. Replacing chemical zinc phosphating with electrolytic calcium phosphating also eliminates heavy metal sludge in phosphating bath resulting in coatings free of heavy metals such as Zn and Ni [4]. Another alternative to zinc phosphate coatings are microporous coatings. Utsunomiya et al. used artificial oxidation in air followed by reduction of oxides in hydrogen atmosphere to create porous

surfaces on steels [7]. Similarly, Arentoft et al. used selective etching to remove one of the two metals in two phase alloy of Sn and Zn, which was electrochemically deposited on surface to develop porous coatings [8]. These small pores act as reservoirs to carry and distribute lubricant during the forming process. Additionally, dry-in-place lubricating systems have been developed to replace phosphate coatings. Hu et al. evaluated three different dry-in-place lubricants and compared it with conventional phosphating lubricant. The study showed mica-type lubricant had comparable friction characteristics to those of the conventional phosphating lubricant at temperature of 210 °C [9].

On the tool side, different hard coatings are used to decrease the friction during the forming process. Development of newer coatings has enabled dry forming without any lubricants. Bobzin et al. developed a new coating system of CrAlN+MoS, where the hard CrAlN matrix is enhanced with Mo and S to provide friction reduction by the formation of a MoS_2 layer under tribological conditions [10]. The developed coating was tested for dry full forward impact extrusion tests and showed no wear and 15% lower punch forces compared to uncoated dies. Likewise, Prieske and Vollersten investigated the use of Chemical Vapour Deposition (CVD) diamond coatings for dry forming of aluminium and showed its suitability for wire drawing [11]. Although these new coatings offer great potential for dry forming, they have not been tested at an industrial scale and might not be effective for PM components due to increased friction conditions due to open pores.

PM processes are well known for high material utilisation and ability to produce near-net shape components [12]. Similar to the porous coatings, the process-induced porosity of PM components can be used as lubricant storage [13]. This eliminates the need for conversion layer coatings and their negative impacts. During the forming process, the lubricant stored in the pores is released, effectively lubricating the surfaces of the tool and the workpiece. Besides, the forming process also compacts the material improving its mechanical properties. Preliminary investigations by Behrens et al. showed that 20% higher forces were required during compression tests of dry PM components compared to the PM components impregnated with lubricant [14]. Furthermore, no cracks were observed in the PM components impregnated with the lubricant in contrast to the dry ones. The compression test also resulted in the reduction of the porosity of the component. Similar investigations on forming behaviour of PM components using compression tests also reported densification of material due to closing of pores [15-17]. The combination of the self-lubrication behaviour of lubricant infiltrated PM products and the compaction of the material during cold forming processes presents a high potential for more ecological manufacturing.

To manufacture defect-free PM components using cold forming processes, it is crucial to design the process taking into consideration the brittleness of the PM components due to its pores. FEM is an efficient tool to reduce time and costs associated with process design. However, detailed knowledge of material behaviour is essential to obtain reliable simulation results. The flow behaviour of the material is a key input for modelling the plastic behaviour during forming. In this paper, the flow behaviour of the PM components is characterised by means of local compression and local tensile tests.

Material and Methods

Steel powder mixture Atomet 1001 (Rio Tinto Metal Powders) was used in this study. Table 1 contains the chemical composition of the powder [18]. The compaction was carried out from both sides (top and bottom) using a multi-axial powder press HPM 200 E2 from SMS Meer. A 130.7 g of powder mixture was used to create a green body by applying a compacting pressure of 353.7 MPa. The green body was then sintered in Gero HTK 8 sintering furnace from Carbolite Gero GmbH & Co. KG under vacuum condition (10^{-3} bar) at 1,000 °C for 60 min. The process resulted in a cylindrical specimen with a diameter of 30 mm and a height of 26.74 mm. The resulting specimen has an absolute geometrical density of 6.839 g/cm^3 with a standard deviation of 0.128% and a relative density of 0.9. The relative density was determined using a spark plasma sintered specimen with a density of 7.6 g/cm^3 as a reference. The resulting density is sufficient to allow lubricant infiltration but not so low that the formability is reduced significantly.

Table 1. Chemical composition of Atomet 1001 in wt% [18].

C	O	S	Mn	Fe
0.004	0.09	0.01	0.18	≥ 99.4

The powder pressing results in inhomogeneous distribution of pores in the specimen due to the effects of friction during pressing [19]. To evaluate the effect of inhomogeneity on flow behaviour due to the porosity distribution, compression and tensile specimens were extracted from various regions of the specimen by wire erosion. The extraction regions of compression and tensile specimens is shown in Fig. 1. To analyse the effect of inhomogeneity in axial direction, the specimens were extracted from three different heights (top, middle, and bottom). For analysing the effect of inhomogeneity in radial direction, specimens were extracted from different radii. For compression tests, specimens were extracted from three radial positions: centre (D0), diameter of 14 mm (D14) and 23 mm (D23). The compression specimens had a diameter of 5 mm and height of 10 mm. For tensile tests, specimens were continuously extracted from one end to another with a thickness of 2 mm.

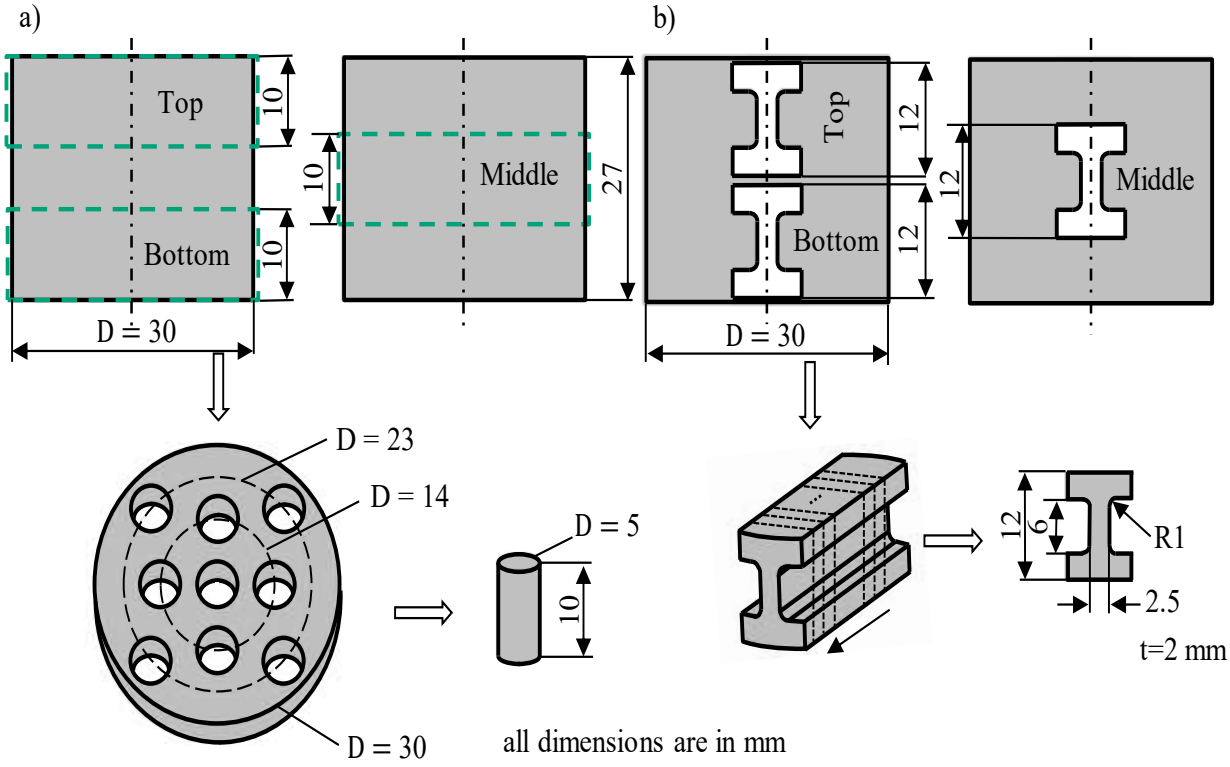

Fig. 1. Extraction regions of a) compression and b) tensile specimens.

The compression tests were carried out in a servo-hydraulic forming simulator DYNSJ5590 from Instron GmbH. The experimental setup and a schematic cross-sectional view are shown in Fig. 2. For testing, the specimen was placed between two punches and then compressed at the velocity of 10 mm/s by moving the lower punch at room temperature to half the initial height. This results in initial strain rate of 1 s^{-1}. The chosen velocity corresponds to the forming process being analysed. The tests were repeated at least three times (three times for D0 and twelve times for D14 and D23). The force F was measured using a strain gauge-based force measuring cell and the length change Δl using inductive path sensor. Since the displacement was measured using the position of the punch rather than directly on the specimen, empty test runs were performed to remove the elastic deformations of the machine from the data.

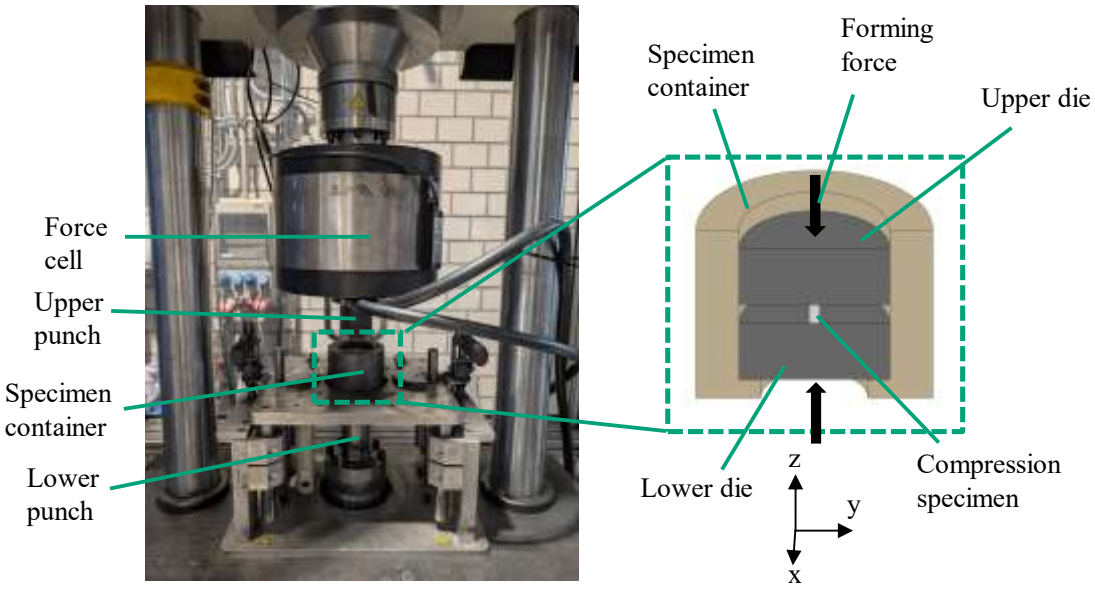

Fig. 2. Test setup for compression test.

The tensile tests were carried out in a quenching and forming dilatometer DIL 805A/D/T from TA Instruments. The tests were performed according to Mohnfeld et al. [20]. A schematic illustration of the test setup is shown in Fig. 3. For testing, the specimen was placed between two specimen holders and tested with a strain rate of 1 s^{-1} at room temperature until fracture. The tests were repeated three times. During the experiments, the force F was measured using force cell and length change Δl was measured using two push rods.

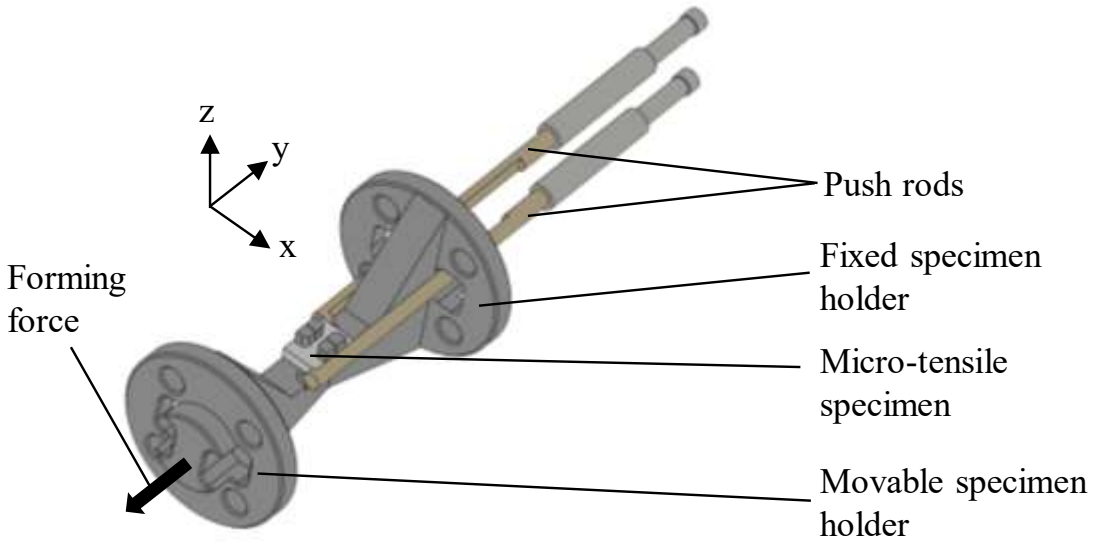

Fig. 3. Schematic of tensile test setup.

The force and length change measured during the experiments were then used to calculate true stress σ and true plastic strain ε_{pl} using Eq. 1 and 2, where A_i is the instantaneous cross-sectional area, l_0 is the initial length of the specimen, and E is the Young's modulus of elasticity.

$$\sigma = \frac{F}{A_i} \tag{1}$$

$$\varepsilon_{pl} = \ln\left(1 + \frac{\Delta l}{l_0}\right) - \frac{\sigma}{E} \tag{2}$$

Results and Discussion

The engineering stress strain curves for compression and tensile test are shown in Fig. 4. For compression, specimen D0 from middle section and D23 from top section were used to represent central and outer region respectively. For comparison of engineering stress, the tensile specimens were selected from similar extraction positions as the compression specimens. For this purpose, a tensile specimen with a radial distance of 0.9 mm was selected from the middle section and taken from the upper section with a radius of 13.08 mm.

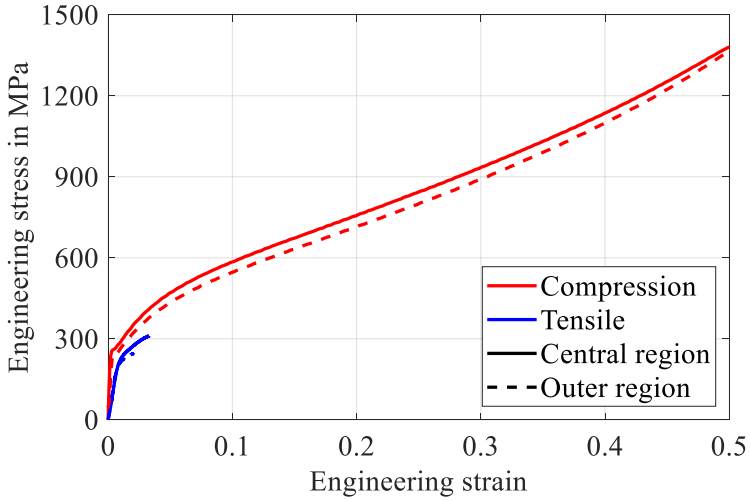

Fig. 4. Engineering stress strain curves for compression and tensile test.

With the compression test, significantly higher deformations up to an engineering strain of 0.5 can be reached compared tensile test for both central and outer region. This can be explained by the different behaviour of the pores present in the specimen during compression and tension [21]. During compression, the pores are closed resulting in the densification of the material that allows material to accommodate high strains. On the contrary, during the tensile test, the pores grow larger severely limiting the ability of material to undergo plastic deformation. Ultimately, the pores act as a source for crack initiation leading to premature fracture of the material. The material also fractures at the maximum engineering stress indicating the brittle nature of material under tension. To evaluate the flow behaviour of the material, flow curves were calculated using Eq. 1 and 2 for the specimens from the different positions of the cylinder. The resulting median flow curves from the compression tests are shown in Fig. 5. The median flow curve is chosen to avoid the influence of outliers for D14 and D23 specimens and to accurately reflect the actual material behaviour. The range of scattering is also plotted for specimens from the middle section. It is determined by subtracting the minimum flow stress from the maximum flow stress and then dividing the result by the median flow stress. Similar ranges of scattering were also obtained for specimen from top and bottom sections. These are not shown to maintain readability of the figure.

In Fig. 5a, flow curves for different radial positions from the middle section of the cylinder are plotted. When comparing the flow behaviour from the different radial positions, slightly lower flow stresses are observed with increasing radial distance from the centre. An explanation could be that during powder compaction, friction at the die wall causes the powder to be loosely packed at the outer region compared to the core [22, 23]. This results in a density gradient along the radius of the cylinder with the highest density in the core. This density gradient causes the higher flow stresses in the specimen from the core compared to the outer regions. Upon closer examination, the disparity in flow stresses between specimens from radial positions D0 and D14 is less pronounced than that between D14 and D23. This suggest that D0 and D14 exhibit similar level of homogeneity, but it decreases between D14 and D23.

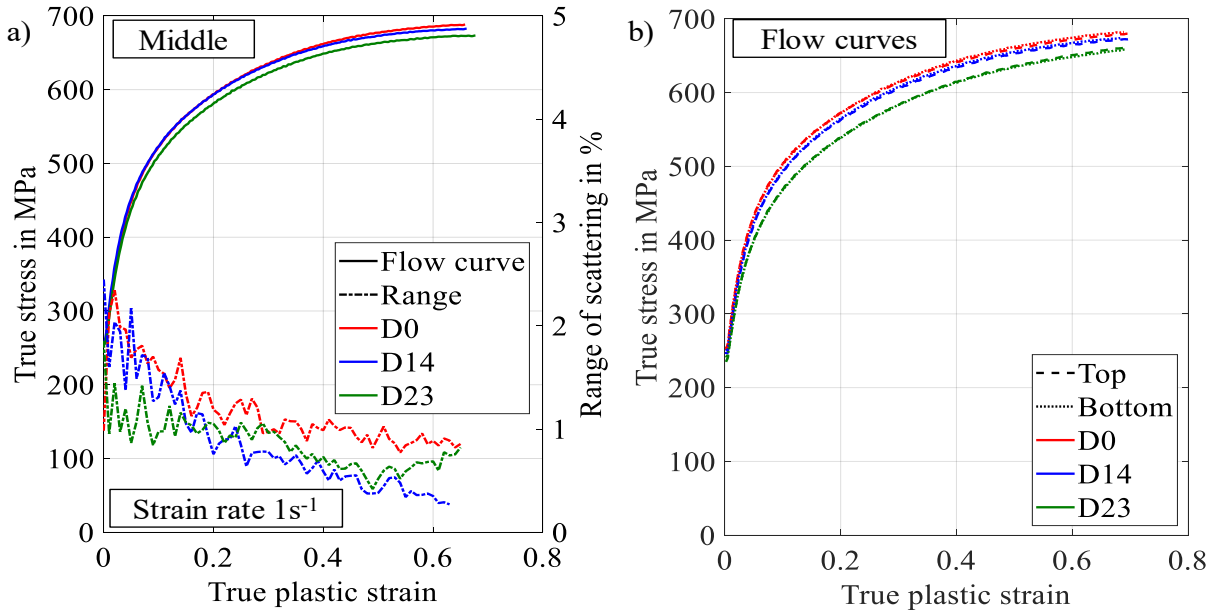

Fig. 5. Flow curves from compression tests for different specimen positions: a) middle, b) top and bottom.

In Fig. 5b, flow curves for different radial positions from the top and bottom sections of the cylinder are shown. Here, a similar behaviour along the radial direction can be seen. A negligible difference in flow stresses is observed when comparing the flow curves from same radial position for top and bottom section. As the powder is pressed from both sides with equal forces, a symmetric specimen is obtained lengthwise. Furthermore, lower flow stresses are observed when comparing with the specimen from the middle section. At a plastic strain of 0.2, deviations of 21.55 MPa (3.62 %) for D0, 29.65 MPa (5 %) for D14, and 42.1 MPa (7.24 %) for D23 can be observed between specimens from middle and top/bottom sections. These discrepancies in flow stresses also align with the porosity measurements reported by Behrens et al., where the porosity at the centre of the cylinder was 4.84 % compared to over 10 % at the outer regions [13]. To compare the flow behaviour under tension and compression, flow curves of specimen from central position of the cylinder are plotted in Fig. 6.

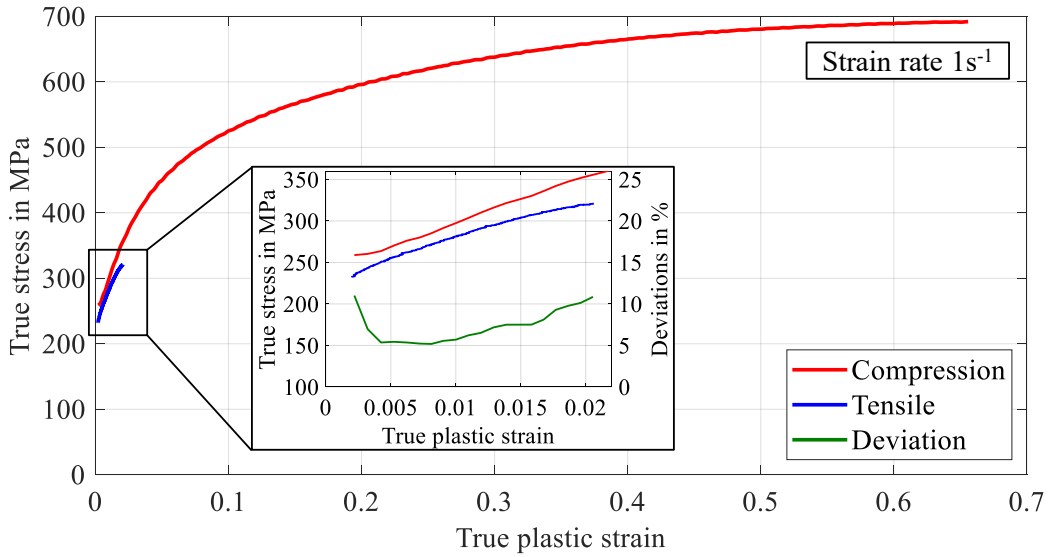

Fig. 6. Material flow behaviour at central position of cylinder under compression and tension.

Under tension, the material yields at a lower flow stress of 232.2 MPa compared to 258.8 MPa under compression. A deviation of above 10 % can be seen in flow stress even for a relatively low plastic strain of 0.02. During tension, pores act as a region for stress concentrations, resulting in

localised yielding of the material at lower stress. In addition, tensile force causes the pores to grow reducing the effective cross-sectional area that withstands the forming force. This causes the material to deform at lower forces resulting in lower flow stresses. On the contrary, compressive forces cause the material to densify through closure of pores resulting in higher yield strength and flow stresses. In Fig. 7, the radial distribution of the tensile strengths and failure strains at different extraction positions are shown. The effect of the inhomogeneous distribution of the pores can be seen here.

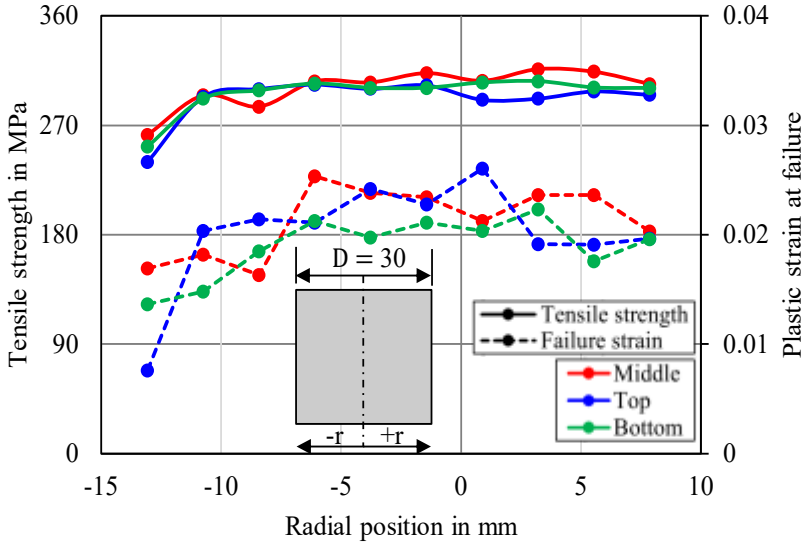

Fig. 7. Tensile strength and failure strain of material at different specimen positions.

The specimen from the outermost radial position of the cylinder shows the lowest tensile strength for specimens from all three axial positions. The remaining specimens from the different radial positions show a similar level of tensile strength at approx. 300 MPa. This shows that the material is homogeneous within a diameter of 20 mm and is increasingly porous between 20 mm and 30 mm. The flow behaviour from the compression tests also demonstrated similar result (compare D23 and D14 in Fig. 5). The porous outer region makes it well-suited for lubricant impregnation. Furthermore, tensile tests also exhibit lower failure strains at the outer region of the cylinder. For the top and bottom sections, the lowest failure strain is observed at the outermost radial position. For the middle section, outermost radial position shows the second lowest failure strain with a value of 0.169 with radius of 8.4 mm showing lowest with a value of 0.163. This brittle behaviour of material especially at the outer region of cylinder needs to be taken into account for designing subsequent forming process.

Summary and Outlook

PM semi-finished products offer great potential for self-lubrication application due to the process related porosity in the material. The inhomogeneity present in the PM components due to the pores results in different material behaviour depending on the region of the workpiece. Higher flow stresses and tensile strength were observed for the specimens from the core as compared to the outer region indicating higher porosity in the outer region. Furthermore, different material behaviour under tension and compression was found, with higher yield strength and flow stresses observed during compression.

In future work, porosity measurements will be performed to validate the differences in mechanical behaviour attributable to local porosity differences. Additionally, the behaviour of pores during compression and tension will be studied using microstructural images. In parallel, the flow behaviour of the PM components will be modelled taking into account the inhomogeneity in porosity. Flow behaviour will also be characterised at different strain rates. Furthermore, for design of defect-free forming process of PM-components, Gurson Tvergaard Needleman (GTN) damage model [24] will be parametrised based on the tensile tests in order to take damage into account during simulation of the forward rod extrusion.

Acknowledgement

Funded by the Deutsche Forschungsgemeinschaft (DFG, German Research Foundation) – 264818458.

References

[1] European Parliament, Council, REACH, EC Regulation No. 1907/2006 of the European Parliament and of the Council, (2006).

[2] N. Karunathilaka, N. Tada, T. Uemori, R. Hanamitsu, M. Fujii, Y. Omiya, M. Kawano, Effect of lubrication and forging load on surface roughness, residual Stress, and deformation of cold forging tools, Metals 9 (2007), 783. https://doi.org/10.3390/met9070783.

[3] N. Bay, The state of the art in cold forging lubrication, Journal of Materials Processing Technology 46 (1994) 19–40. https://doi.org/10.1016/0924-0136(94)90100-7.

[4] N. Bay, A. Azushima, P. Groche, I. Ishibashi, M. Merklein, M. Morishita, T. Nakamura, S. Schmid, M. Yoshida, Environmentally benign tribo-systems for metal forming, CIRP Annuals 59 (2010) 760-780. https://doi.org/10.1016/j.cirp.2010.05.007.

[5] M. Gariety, G. Ngaile, T. Altan, Evaluation of new cold forging lubricants without zinc phosphate precoat, Int. Journal of Machine Tools and Manufacture 47 (2007) 673-681. doi:10.1016/j.ijmachtools.2006.04.016.

[6] N.J. Bjerrum, E. Christensen, T. Steenberg, Method for electrochemical phosphating of metal surfaces, Danish patent, No. 0910/96/US patent, US 6,346,186 B1. (1996/2002).

[7] H. Utsunomiya, S. Kawajiri, N. Takahira, J. Miyamoto, T. Sakai, T. Tanaka, Porosification of Steel Surface—New Lubrication System for Cold Forging, in Azushima A, (Ed.) Proceed, 3rd Int. Conf. on Tribology in Manuf. Process (2007) 363–72.

[8] M. Arentoft, N. Bay, P.T. Tang, J. D. Jensen, A new lubricant carrier for metal forming, CIRP Annuals – Manufacturing Technology 58 (2009) 243-246. doi:10.1016/j.cirp.2009.03.062.

[9] C. Hu, S. Osaki, B. Cai, M.Aoyama, K. Dohda, Evaluation of dry-in-place lubricants for cold forging by using an optimal steady combined forward and backward extrusion testing method, Friction 11 (2023) 1862-1876. https://doi.org/10.1007/s40544-022-0717-3.

[10] K. Bobzin, T. Brögelmann, N. C. Kruppe, T. Bergs, P. Mattfeld, D. Trauth, R. Hild, D. C. Hoffmann, PVD coated tools and surface-structured workpieces in dry cold forming of steel, Defect and Diffusion Forum 404 (2020) 19-27. https://doi.org/10.4028/www.scientific.net/DDF.404.19.

[11] M. Prieske, F. Vollersten, Polished diamond coatings for dry tapering of aluminum, Dry Metal Forming Open Access Journal 6 (2020) 334-353.

[12] A. Panda, J. Dobransky, M. Jancik, I. Pandova, M. Kacalova, Advantages and effectiveness of the powder metallurgy in manufacturing technologies, Metalurgija 57 (2018) 353-356.

[13] B.-A. Behrens, K. Brunotte, D. Bohr, Experimental investigation of endogenous lubrication during cold upsetting of sintered powder metallurgical components, Key Engineering Materials 767 (2018) 163-170. https://doi.org/10.4028/www.scientific.net/KEM.767.163.

[14] B.-A. Behrens, K. Brunotte, D. Bohr, Ecological lubrication in cold forming of sintered powder metallurgical components, Dry Metal Forming Open Access Journal 4 (2018) 68-73.

[15] C.-C. Huang, J.-H Cheng, An investigation into the forming limits of sintered porous materials under different operational conditions, Journal of Materials Processing Technology 148 (2004) 382–393. doi:10.1016/j.jmatprotec.2003.10.024.

[16] A. P. Mohan Raj, N. Selvakumar, Deformation behaviour of sintered Fe-C-Mn composite During cold upset forming. Materials and Manufacturing Processes 26 (2011) 1388– 1392. doi: 10.1080/10426914.2010.544820.

[17] U. J. Prasanna Kumar, P. Gupta, A. K. Jha, and D. Kumar, Closed die deformation behaviour of cylindrical iron–alumina metal matrix composites during cold sinter forging, J. Inst. Eng. India Ser. D 97 (2016) 135–151. doi: 10.1007/s40033-015-0089-1.

[18] Rio Tinto Metal Powders, ATOMET 1001 Data Sheet, (2025, Dec 14). Information on https://qmp-powders.com/wp-content/uploads/ATOMET_1001.pdf.

[19] M. Zhou, S. Huang, Y. Lei, J. Hu, S. Yan, F. Zou, Investigation on compaction behaviors of Ag35Cu32Zn33 mixed metal powders under cold die compaction, Journal of Advanced Mechanical Design, Systems, and Maufacturing 12 (2018). https://doi.org/10.1299/jamdsm.2018jamdsm0037.

[20] N. Mohnfeld, A. Dewidar, K. Qarbi, H. Wester, F. P. Schäfke, A. Verschinin, H. J. Maier, S. Barton, C. Klose, J. Uhe, Non-destructive and mechanical characterisation of bond quality of co-extruded titanium-aluminium profiles, Advanced Engineering Materials 27 (2024). https://doi.org/10.1002/adem.202401716.

[21] L. Bertini, V. Fontanari, G. Straffelini, Tensile and bending behaviour of sintered alloys: Experimental results and modelling, Journal of Engineering Materials and Technology 120 (1998) 248-255. https://doi.org/10.1115/1.2812351.

[22] P. R. Brewin, O. Coube, D. T. Gethin, H. Hodgson, S. Rolland, Applications in Industry, in P.R. Brewin, O. Coube, P. Doremus, J. H. Tweed (Eds.), Modelling of Powder Die Compaction, Springer, London, 2008, pp. 243-258.

[23] W. Wang, H. Qi, O. Liu, Y. Zhao, H. Chang, Numerical simulation of densification of Cu-Al mixed metal powder during axial compaction, Metals 8 (2018) 537. https://doi.org/10.3390/met8070537.

[24] V. Tvergaard, A. Needleman, Analysis of the cup-cone fracture in a round tensile bar, Acta Metallurgica 32 (1984) 157-169. https://doi.org/10.1016/0001-6160(84)90213-X.

The publication of this article was funded by the Leibniz Universität Hannover (LUH) / Technische Informationsbibliothek (TIB)